

# Robust control of uncertain cylinder wake flows based on robust reduced order models

L. Mathelin <sup>a,\*</sup> & O.P. Le Maître <sup>b,c</sup>

<sup>a</sup>*LIMSI-CNRS, BP 133, F-91403 Orsay, France.*

<sup>b</sup>*LIMSI-CNRS, BP 133, F-91403 Orsay, France.*

<sup>c</sup>*DEN/DM2S/SFME, Centre d'Etudes Nucléaires, Saclay, France.*

---

## Abstract

A technique for the construction of robust orthogonal flow bases, to be used for model reduction and flow control, is proposed. The construction accounts for the dependence of the flow structures with the control and variability in the flow conditions. Numerical examples, for the two-dimensional flow around a circular cylinder in laminar regime, are provided to demonstrate the robust character of the resulting reduced basis. The control of the flow is then considered with the objective of reducing the body drag in a full information framework, by blowing/suction at the cylinder surface. Different control strategies are considered, some being also robust in the sense that they incorporate a variability in the flow conditions (Reynolds number). The improvements brought by the robust basis and robust control strategies is evidenced for the control of the reduced model and, more important, when the control laws determined for the reduced model are applied to the fully detailed flow model (DNS).

*Key words:* robust control, POD, reduced model, uncertainty propagation, adjoint formulation.

---

## 1 Introduction

Today's course on performance and efficiency in all areas of human activities finds a particular resonance in the field of fluid mechanics where optimization and control has been the subject of a continuous research effort since

---

\* Corresponding author. Tel: 33-169 85 80 69; fax: 33-169 85 80 88.

*Email addresses:* mathelin@limsi.fr (L. Mathelin), olm@limsi.fr (O.P. Le Maître).

the beginning. In addition to the experimental approach, engineers now also rely on numerical simulations of sophisticated physical models and numerical methods. Though now more accurate and reliable, the simulations and/or experiments still require a significant time to run and the control process remains a difficult part. One thus has to make a compromise between the available computational power or experimental facilities and the required accuracy in the control law derivation process. Among different approaches to achieve a good compromise, the model reduction is one of the most popular. It basically consists in projecting the original system onto low-dimensional manifolds while retaining the essential features required for fidelity of the dynamics and reliably optimizing. While there exists different strategies for reducing the original problem, the Proper Orthogonal Decomposition (POD) first proposed by Lumley [17] is one of the most widely used. Its most appealing feature is that the resulting orthogonal basis is optimal for the energy in the ergodic sense: it is the best (highest convergence rate) representation to capture the flow energy which makes it a very attractive ingredient for the derivation of reduced-order dynamical models, see [12] among many others. The initial large scale problem is thus restricted to a low number of variables allowing for a fast and easy handling and making this approach a good candidate for flow control applications.

To make the numerical model reduction accurate and realistic enough to be reliably applied to a real-world configuration, one has to account for the unmodelled perturbations to the ideal system considered. More specifically, the real system is likely to have a slightly different dynamics and to experience different conditions from the ones considered for the reduced basis derivation. This leads to the need for a *robust* model reduction as well as a *robust* control of the resulting dynamical system. Just as the reduced model has to be robust against non-modelled dynamics and boundary conditions, the control must account for poorly known operating parameters to remain efficient when applied to a real system subjected to uncertain parameters and perturbations. Both these issues are addressed in this paper for the flow around a circular cylinder in cross-flow at low Reynolds numbers. Specifically, the control of the flow in a full information framework is considered with the objective of body drag reduction by blowing/suction at the cylinder surface.

The manuscript is organized as follows: the context of the model reduction is presented in Section 2 and the emphasis is put on the derivation of a reduced basis which remains consistent and as accurate as possible throughout the a range of control process and flow conditions. The flow model is presented in Section 3 together with the performance of the robust reduced basis. After a theoretical presentation, the application of the adjoint-based robust reduced model in the context of optimal and robust control is addressed in Section 4 and 5 respectively.

## 2 Construction of robust bases

### 2.1 Robust bases

In a controlled reduced model perspective, it is important to ensure that the state space spanned by the reduced model is representative of the state space in which the controlled flow evolves. In other words, it is required that the basis derived from the model reduction technique remains appropriate throughout the control process of the flow. Since the control law is not known *a priori*, a robust, extended, reduced basis for the flow is needed in the sense that it must remain valid for any control law belonging to a prescribed range, the control space. The relevance of the reduced model basis to flow control applications has long been identified as a difficulty and received attention from many authors. While the POD basis constructed from the non-controlled flow may still be relevant in certain controlled configurations, this remains limited to a narrow control parameter range and to mild changes in the flow structure. To widen the field of application of reduced models to larger control ranges and having a deeper impact on the flow structure and dynamics, [29] and [11] proposed to use the spatial modes of the non-controlled flow POD basis, but to correct their dynamics using information extracted from the actual controlled flow field. Other techniques include the so-called shift modes [22] which complement the non-controlled flow POD basis to achieve a better representation of the controlled flow dynamics. These shift modes are derived from the difference between the time-averaged flow at prescribed constant control conditions and the corresponding steady flow solution, and are subsequently orthogonalized with regard to the POD modes of the non-controlled flow. In [6, 9] and more recently in [21, 22] this shift mode technique has been used successfully for flow control.

Another approach consists in defining a trust-region in the control parameter space over which the reduced model is deemed representative of the flow dynamics. See [7] for a comprehensive introduction to the trust-region ideas. Whenever the control parameter leaves the trust region, a new reduced model is constructed to better account for the flow dynamics in the actual range of operating conditions.

Reduced bases interpolation is another mean to construct a reduced model valid over the whole control range. In [3] cubic polynomials are used to interpolate the flow dynamics for different control parameter and subsequently construct a local POD basis and reduced model. A strategy based on the interpolation of flow correlation matrices, corresponding to different control parameter values, was proposed in [8] and successfully applied to control the instabilities in the wake of a square cylinder.

While reasonably efficient, these techniques either stand on heuristic grounds or require additional on-the-fly calculations as the flow dynamics is affected by the control. Because performing significant calculations as the flow is modified by control may not be desirable, in particular in the real-time control context, a truly robust *a priori* reduced model is required. Such model would involve a POD basis that need not to be updated as the control is applied and that should thus remain relevant for the controlled as well as for the non-controlled flow dynamics. Different works have investigated this issue with the common idea to enrich the set of uncontrolled flow fields (snapshots) used to derive the POD basis by incorporating snapshots corresponding to different control parameter values. Specifically, the POD modes must be extracted from the richest and most representative set of flow dynamics possible within the control range. In [24] as well as in [28], a series of snapshots of the uncontrolled flow is combined with another series of snapshots of the flow submitted to the largest control intensity attainable. They assume that the flow dynamics for intermediate control intensity are naturally encompassed. Similarly, [18] uses two sets of snapshots for the lowest and highest value of their control parameter and successfully simulates the flow for intermediate control values. In a similar spirit, some authors have applied a prescribed time-dependent control during the snapshots acquisition sequence to trigger some additional frequencies and add control-induced transients in the flow dynamics (see [32] and [1] among others).

The question which then arises is how to select the control values to enrich the flow dynamics to be reduced? Most authors used control values evenly distributed in the control parameter range while [4] used the Voronoi tessellation to derive a strategy for choosing the control parameter values when constructing the reduced basis. This method essentially consists in defining local trust regions in the sense that the originally large snapshots set is “coarsened” to retained only snapshots representative of the flow dynamics in some neighborhood of the control range. The naive image would be to retain every few snapshots and assume the selected ones are representative enough of the discarded ones. The Voronoi tessellation has a more rigorous basis as it leads to retain the most representative (centroidal) information within a region of the control parameter range, which size is set from a suitable norm. In practice, it leads to retain a coarsened set of snapshots to be orthogonalized, while the POD method retains the largest eigenvectors of the auto-correlation matrix of the whole set of snapshots.

## 2.2 Proposed method

To construct the robust basis, we propose to treat the control as a random quantity. To this end, we denote  $\mu$  the random control vector and introduce

an abstract probability space  $(\Theta, \mathcal{B}, dP)$ ,  $\Theta$  being the set of elementary outcomes  $\theta$ ,  $\mathcal{B}$  the  $\sigma$ -algebra of the events and  $dP$  a probability measure. We denote  $L_2(\Theta, dP)$  the space of second order random variables defined on the probability space. The random control  $\mu(\theta)$  acts on the flow which is thus dependent on the outcome  $\theta$ . In the following, we seek for a reduced robust basis for the representation of the vorticity field of a two dimensional flow. The method can however be extended to the three-dimensional case and the representation of flow velocity fields.

We denote  $\omega$  the vorticity field of the flow:

$$\omega : (x, t, \theta) \in (\Omega_x \times T_w \times \Theta) \mapsto \omega(x, t, \theta) \in \mathbb{R}, \quad (1)$$

where  $\Omega_x$  is the flow domain and  $T_w$  the time-interval of the analysis. We assume  $\omega(x, t, \theta) \in L_2(\Theta, dP)$  for all  $x \in \Omega_x$  and  $t \in T_w$ . We define the inner product on  $L_2(\Omega_x)$ ,

$$(f; g)_{\Omega_x} \equiv \int_{\Omega_x} f(x) g^*(x) dx = (g; f)_{\Omega_x}^*, \quad (2)$$

where  $*$  denotes the complex conjugate, and the ensemble average over the time interval  $T_w$

$$\langle f(x, t, \theta) \rangle_{T_w} \equiv \frac{1}{T_w} \int_{T_w} \int_{\Theta} f(x, t, \theta) dP(\theta) dt. \quad (3)$$

The vorticity field can be decomposed into a mean and fluctuating fields:

$$\omega(x, t, \theta) = \bar{\omega}(x) + \omega'(x, t, \theta), \quad (4)$$

where

$$\bar{\omega}(x) = \langle \omega(x, t, \theta) \rangle_{T_w}, \quad \langle \omega'(x, t, \theta) \rangle_{T_w} = 0. \quad (5)$$

Following [12], an optimal basis, in the energy sense, for the representation of the stochastic process  $u$ , is the set of functions  $\varphi_i : x \in \Omega_x \mapsto \varphi_i(x) \in \mathbb{R}$  satisfying:

$$\varphi \mid \epsilon = \frac{\langle |(\omega'; \varphi)_{\Omega_x}|^2 \rangle_{T_w}}{\|\varphi\|^2} = \max_{\varphi} \{\epsilon\}, \quad \varphi_i \in L_2(\Omega_x), \quad (6)$$

with  $\|\cdot\|$  the usual norm on  $L_2(\Omega_x)$ . The basis vectors are subjected to normalization:  $\|\varphi_i\| = 1$ .

It is convenient to rewrite the problem under a non-constrained form by introducing the Lagrangian operator  $\mathcal{L}$ ,

$$\mathcal{L}(\varphi) \equiv \langle |(\omega'; \varphi)_{\Omega_x}|^2 \rangle_{T_w} - \lambda (\|\varphi\|^2 - 1), \quad (7)$$

where  $\lambda$  is a Lagrange multiplier of the normalization constraint. The Lagrangian has to be maximized for  $\varphi$ , that is  $d\mathcal{L}(\varphi)/d\varphi = 0$ , which expresses under a Fréchet derivative form as

$$\left. \frac{d\mathcal{L}(\varphi + \delta\phi)}{d\delta} \right|_{\delta=0} = 0, \quad \delta \in \mathbb{R}, \quad \forall \phi \in L_2(\Omega_x). \quad (8)$$

This guarantees that whatever  $\delta$  tending to zero, the derivative vanishes, yielding

$$\left. \frac{d}{d\delta} \left[ \langle |(\omega'; \varphi + \delta\phi)_{\Omega_x}|^2 \rangle_{T_w} - \lambda (\|\varphi + \delta\phi\|^2 - 1) \right] \right|_{\delta=0} = 0, \quad (9)$$

so

$$\left. \frac{d}{d\delta} \left[ \langle (\omega'; \varphi + \delta\phi)_{\Omega_x} (\varphi + \delta\phi; \omega')_{\Omega_x} \rangle_{T_w} - \lambda ((\varphi + \delta\phi)(\varphi + \delta\phi) - 1) \right] \right|_{\delta=0} = 0, \quad (10)$$

which simplifies in

$$\langle (\omega'; \phi)_{\Omega_x} (\varphi; \omega')_{\Omega_x} \rangle_{T_w} - \lambda (\varphi; \phi)_{\Omega_x} = 0, \quad \forall \phi \in L_2(\Omega_x). \quad (11)$$

As  $\phi$  is arbitrary, this equation can be rearranged in

$$\left\langle \int_{\Omega_x} \omega'(x, t, \theta) \varphi(x') \omega'^*(x', t, \theta) dx' \right\rangle_{T_w} - \lambda \varphi(x) = 0. \quad (12)$$

Let  $R : \varphi \in L_2(\Omega_x) \mapsto R\varphi \in L_2(\Omega_x)$  be the operator defined as:

$$R\varphi(x) = \left\langle \int_{\Omega_x} \omega'(x, t, \theta) \omega'^*(x', t, \theta) \varphi(x') dx' \right\rangle_{T_w} \quad (13)$$

Eq. (12) now simplifies to:

$$R\varphi(x) = \lambda \varphi(x). \quad (14)$$

It can be shown that:

$$(R\varphi(x); \phi(x))_{\Omega_x} = (\varphi(x); R\phi(x))_{\Omega_x}, \quad \forall \varphi, \phi \in L_2(\Omega_x). \quad (15)$$

The operator  $R$  is thus linear, self-adjoint and positive on  $L_2(\Omega_x)$ .  $R$  being self-adjoint, its eigen-functions are real vectors and form an orthogonal set:

$$\int_{\Omega_x} \varphi_i(x) \varphi_j(x) dx = \|\varphi\|^2 \delta_{ij} = \delta_{ij} \quad (16)$$

where  $\delta_{ij}$  is the Kronecker delta. Further, the eigen-functions define a basis onto which the vorticity  $\omega$  can be decomposed:

$$\omega(x, t, \theta) = \bar{\omega}(x) + \sum_{i=1}^{\infty} a_i(t, \theta) \varphi_i(x) \quad (17)$$

where

$$a_i(t, \theta) = \int_{\Omega_x} \omega'(x, t, \theta) \varphi_i(x) dx. \quad (18)$$

Identifying  $\omega$  in Eq. (12) with its expansion, it follows:

$$\langle a_i(t, \theta) \omega'(x, t, \theta) \rangle_{T_w} - \lambda_i \varphi_i(x) = 0. \quad (19)$$

Multiplying both side of this equation by the  $\omega'(x, t, \theta)$  and integrating over  $\Omega_x$ , it comes:

$$\begin{aligned} & \int_{\Omega_x} \omega'(x, t, \theta) \langle a_i(t', \theta') \omega'(x, t', \theta') \rangle_{T_w} dx \\ &= \int_{\Omega_x} \omega'(x, t, \theta) \left[ \frac{1}{T_w} \int_{T_w} \int_{\Theta} a_i(t', \theta') \omega'(x, t', \theta') dP(\theta') dt' \right] dx \\ &= \frac{1}{T_w} \int_{T_w} \int_{\Theta} \left( \int_{\Omega_x} \omega'(x, t, \theta) \omega'(x, t', \theta') dx \right) a_i(t', \theta') dP(\theta') dt' \\ &= \lambda_i \int_{\Omega_x} \omega'(x, t, \theta) \varphi_i(x) dx \\ &= \lambda_i a_i(t, \theta). \end{aligned} \quad (20)$$

We define the random operator  $\mathcal{R} : (t, \theta; t', \theta') \in (\Omega_x \times T_w \times \Theta)^2 \mapsto L_2(\Theta, dP; T_w)$  as

$$\mathcal{R}(t, \theta; t', \theta') \equiv \int_{\Omega_x} \omega'(x, t', \theta') \omega'(x, t, \theta) dx, \quad (21)$$

so we end up with the generalized stochastic eigen-problem for the random functions  $a_i(t, \theta)$ :

$$\langle \mathcal{R}(t, \theta; t', \theta') a_i(t', \theta') \rangle_{T_w} = \lambda_i a_i(t, \theta). \quad (22)$$

Remarking that  $\mathcal{R}(t, \theta; t', \theta') = \mathcal{R}(t', \theta'; t, \theta)$ , the eigenvalues in Eq. (22) are all real and positive, and the eigenvectors  $a_i(t, \theta)$  form an orthogonal set in the ensemble average sense:

$$\langle a_i; a_j \rangle = \langle a_i(t, \theta) a_j(t, \theta) \rangle_{T_w} = \lambda_i \delta_{ij}. \quad (23)$$

Finally, the basis functions can then be determined from:

$$\varphi_i(x) = \langle a_i(t, \theta) \omega'(x, t, \theta) \rangle_{T_w}. \quad (24)$$

### 2.3 Implementation

The derivation of the basis just presented above can in fact be extended to situations where not only the control  $\mu$  is considered as random but also some operating conditions. Specifically, in designing a control strategy for a fluid

flow, one must bear in mind that external conditions applied to the system are not always very well characterized and are likely to fluctuate. The control strategy and the model reduction must hence account for this variability of what can be considered as external parameters of the system. In this paper, the major operating parameter is the Reynolds number  $Re$  of the flow. The previous methodology can accommodate with uncertainty in operating conditions, by considering them random as well. Consequently, we denote  $\chi(\theta)$  the random control vector augmented of the random flow parameters.

The main difficulty of the proposed method is the estimation of ensemble averages. To this end, we assume that the random control and operating conditions vector  $\chi$  is parameterized by a finite set of independent real-value random variables  $\{\xi_i, i = 1, \dots, N\}$  with prescribed probability density functions:

$$\chi(\theta) = \chi(\xi_1(\theta), \dots, \xi_N(\theta)). \quad (25)$$

We denote  $p_i(\xi_i)$  the probability density function of  $\xi_i$ . Due to the independence of the  $\xi_i$  their joint density is

$$p_\xi(\xi_1, \dots, \xi_N) = \prod_{i=1}^N p_i(\xi_i), \quad (26)$$

and we denote  $(\Omega_\xi, \mathcal{B}_\xi, p_\xi)$  the associated probability space where  $\Omega_\xi$  is the range of  $\xi$ . On the image space, we have for any random variable  $f(\theta) = f(\xi(\theta))$ . Consequently, the ensemble average has for expression in the image space

$$\begin{aligned} \langle f(t, \theta) \rangle_{T_w} &= \frac{1}{T_w} \int_{T_w} \int_{\Theta} f(t, \xi_1(\theta), \dots, \xi_N(\theta)) dP(\theta) dt \\ &= \frac{1}{T_w} \int_{T_w} \int_{\Omega_\xi} f(t, \xi_1, \dots, \xi_N) p_\xi(\xi_1, \dots, \xi_N) d\xi dt. \end{aligned} \quad (27)$$

The  $N$ -dimensional integration over  $\Omega_\xi$  can be performed by different means (*e.g.* sampling techniques, Monte Carlo, ...). Here we rely on coarse quadrature schemes, *i.e.* cubature schemes, based on the Smolyak formula [23, 25, 31]. These formulas are obtained by a coarse tensorization of 1-D Gauss' quadrature formulas for the integration with weights  $p_i$ . Denoting  $N_q$  the number of quadrature points  $\xi^q = (\xi_1^q, \dots, \xi_N^q)$  and  $w_q$  the associated weights, Eq.(27) becomes

$$\langle f(t, \theta) \rangle_{T_w} \approx \sum_{q=1}^{N_q} w_q \frac{1}{T_w} \int_{T_w} f(t, \xi^q) dt \quad (28)$$

This cubature rule is used to compute the mean vorticity field, while the eigenvalue problem is written on the set of integration points:  $\forall k = 1, \dots, N_q$ ,

$$\sum_{q=1}^{N_q} w_q \frac{1}{T_w} \int_{T_w} \mathcal{R}(t, \xi^k; t', \xi^q) a_i(t', \xi^q) dt' = \lambda_i a_i(t, \xi^k), \quad (29)$$

where

$$\mathcal{R}(t, \xi^i; t', \xi^j) = \int_{\Omega_x} \omega'(x', t', \xi^i) \omega'(x', t, \xi^j) dx'. \quad (30)$$

In the previous expression,  $\omega'(x, t, \xi^i)$  is the deterministic vorticity field for the deterministic operating and control conditions  $\chi = \chi(\xi^i)$ . Finally, the eigen-modes are given by

$$\varphi_i(x) = \sum_{q=1}^{N_q} \frac{w_q}{\lambda_i T_w} \int_{T_w} a_i(t, \xi^q) \omega'(x, t, \xi^q) dt. \quad (31)$$

### 3 Example of robust basis

#### 3.1 Flow solver

The model reduction technique is now applied to a fluid flow to investigate its performance and accuracy. The 2-D incompressible flow around a circular cylinder of diameter  $D$  submitted to a uniform incident flow with constant velocity  $U_\infty$  is considered at a nominal Reynolds number  $Re_0 = U_\infty D/\nu = 200$  with  $\nu$  the kinematic viscosity. For this Reynolds number, the wake of the uncontrolled flow exhibits a periodic vortex shedding pattern. The Reynolds number is assumed to be uniformly distributed in the  $\Omega_{Re} = [180; 220]$ -range. The control is also considered and it is achieved by uniformly injecting or aspirating some fluid through the porous cylinder surface, hence introducing a non-zero normal velocity at its surface. In this section of the paper the blowing/suction intensity, denoted  $\mu$  is time-independent and is given a uniform probability hypothesis onto the range  $\Omega_\mu = [-0.2; 0]$ .

The flow is simulated by solving the Navier-Stokes equations, here considered in their dimensionless  $\psi - \omega$  form (stream function - vorticity) [13]. For any  $\{\mu, Re\} \in \Omega_\mu \times \Omega_{Re}$ , we solve:

$$\left\{ \begin{array}{l} \frac{\partial \omega}{\partial t} + \mathbf{u} \cdot \nabla \omega = \frac{1}{Re} \nabla^2 \omega, \quad (a) \\ \nabla^2 \psi = -\omega, \quad (b) \\ \mathbf{u} = \nabla \wedge (\psi \mathbf{e}_z), \quad (c) \\ \omega \mathbf{e}_z = \nabla \wedge \mathbf{u}, \quad (d) \end{array} \right. \quad (32)$$

together with the boundary conditions on the cylinder surface:

$$\begin{aligned} \mathbf{u} \cdot \boldsymbol{\tau} &= 0, \\ \mathbf{u} \cdot \mathbf{n} &= \mu. \end{aligned} \quad (33)$$

with  $\mathbf{u}$  the fluid velocity,  $\mathbf{e}_z$  the direction normal to the 2-D  $\{x, y\}$  plane of the flow. Vectors  $\boldsymbol{\tau}$  and  $\mathbf{n}$  are the tangential and normal vector to the cylinder surface respectively.

The O-type numerical domain is  $30D$  in diameter around the cylinder, comprising 180 cells both in the radial and the azimuthal directions, leading to a  $180 \times 180$ -cell grid. The governing equations are solved using a second-order centered finite-difference scheme for the linear terms while the non-linear terms (convection) are discretized with a fourth-order up-winded scheme. The time stepping is carried-out through second order Euler scheme and the generation of snapshots covers several vortex-shedding periods (of about 9 time units):  $T_w = 200$ .

### 3.2 Robust basis characterization

To allow comparisons with the modes issued from standard POD, the first POD modes of the robust basis are plotted in figure 1. While most of them exhibit usual patterns, qualitatively corresponding to the well-known POD modes for this flow configuration, some modes are unfamiliar. In particular, mode 1 and 4 have a near cylinder-flow focused pattern and do not seem to have a major contribution to the rest of the flow. Those modes actually correspond to some “correction” accounting for the change of flow structure when the incident flow Reynolds number and/or the applied control intensity through the cylinder surface vary. For a particular value of  $\{Re, \mu\}$ , time-evolution of those modes is not zero-centered but rather provide a constant “correction” to the base flow while the remaining modes account for the time-varying flow and provide the vortex-shedding pattern. However, their ensemble average  $\langle \cdot \rangle_{T_w}$  is indeed close to zero. Those modes are very similar to the so-called “shift modes” described in [6], [9] [22], though derived from a very different procedure. No post Gram-Schmidt orthogonalization procedure is

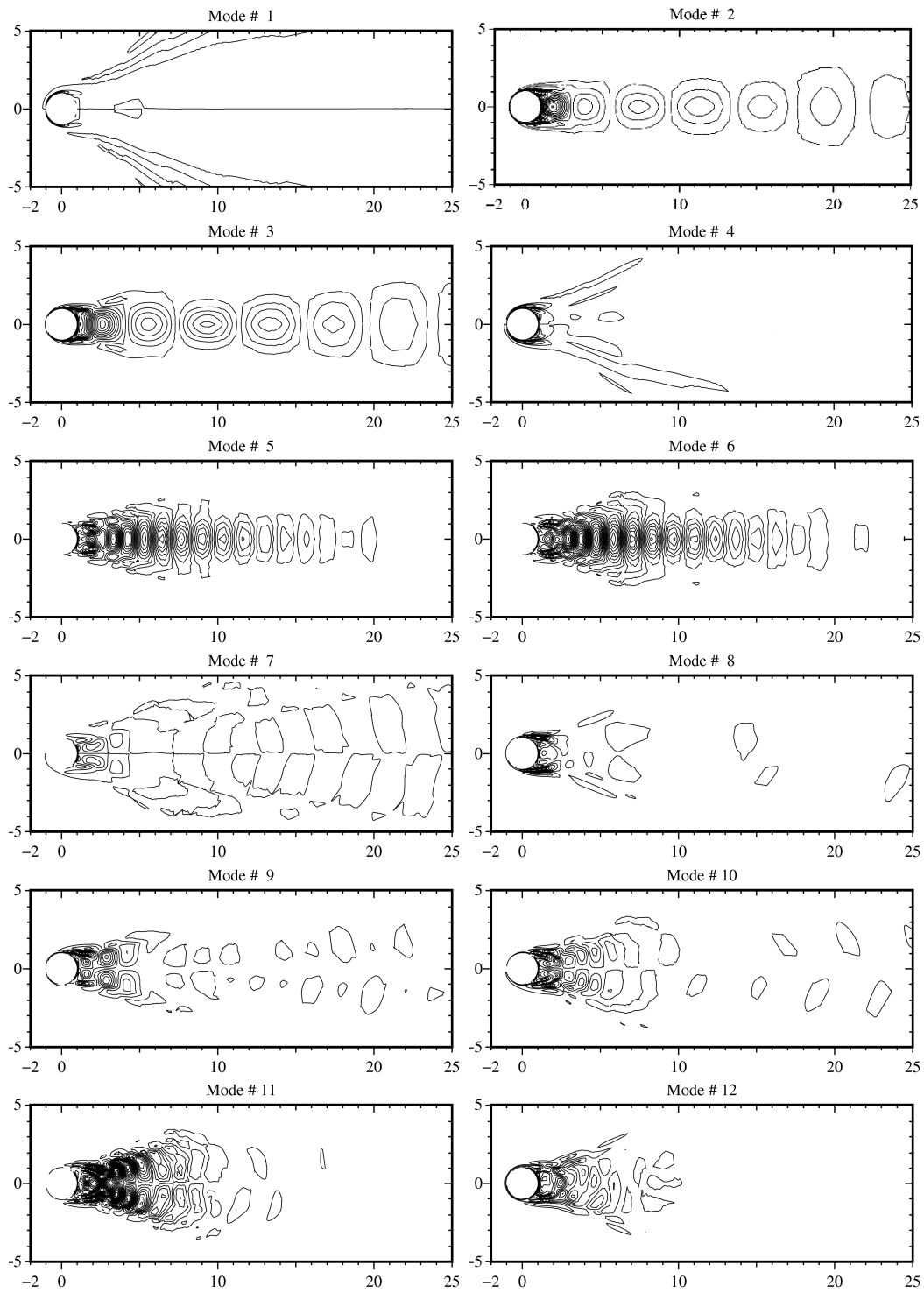


Fig. 1. First POD modes of the vorticity field  $\omega'$ , computed with the robust basis method and  $Re \in [180; 220]$ . Modes are sorted by decreasing eigen values (see spectrum in Fig. 2).

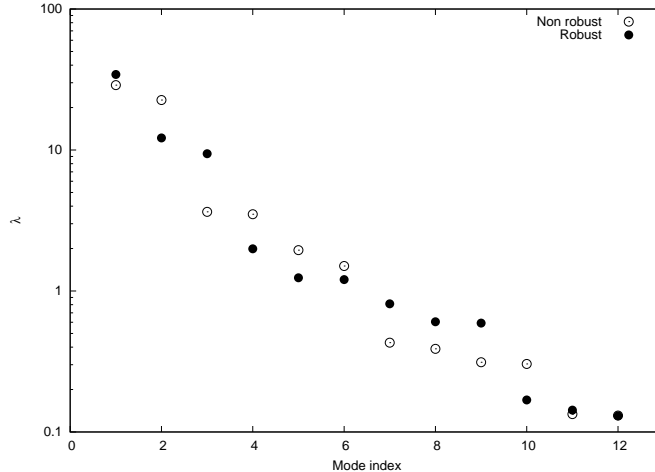


Fig. 2. Spectrum of eigenvalues for robust and non-robust POD bases.

necessary here as the modes are altogether determined from a unique generalized eigen-problem. Further, they are not specific of a particular shift between the reference flow and the flow of interest but they rather are adapted, in the mean sense, to the *full* control and Reynolds range, making the proposed method more self-contained.

The construction of the robust basis does not take advantage of the flow periodicity and the resulting POD modes are hence not exactly symmetric / antisymmetric with respect to the symmetry axis of the flow. Indeed, the vortex shedding frequency varies both with the Reynolds number and the control intensity and no unique, well defined, flow period can thus be identified over the range of parameters.

Figure 2 shows the first eigenvalues for the robust ( $Re \in [180; 220], \mu \in [-0.2; 0]$ ) and the classical POD basis constructed on the flow for  $Re = 200, \mu = -0.1$ . It is observed that the robust basis has eigen-values converging with essentially the same rate as the classical POD basis (non robust). One can further appreciate that, except the “correction” modes, the robust and classical POD bases exhibit the familiar pattern of pairs of eigenvalues, characteristic of propagating flow fields. Note also that the fast decay of the eigenvalues ( $\lambda_1/\lambda_{10} \simeq 200$ ) allows to retain only a limited number  $N_R$  of modes to construct a reduced model, while accounting for almost all the flow energy. In fact, for  $N_R = 12$ , one retains  $\sum_{i=1}^{N_R} \lambda_i / \sum_{i=1}^{\infty} \lambda_i \simeq 99.6$  % of the flow energy.

### 3.3 Application to a reduced model

#### 3.4 Reduced basis performance

The performance of the robust basis derived in section 2 is investigated through comparisons with non-robust classical POD modes. The performance is measured in terms of amount of flow energy accounted for by the modes for both a controlled and non-controlled flow. The “error”  $E_\omega$  due to the reduced basis is quantified according to:

$$E_\omega^2 = \frac{\|\omega_{DNS} - \omega_{POD}\|^2}{\|\omega_{POD}\|^2} \quad (34)$$

where  $\omega_{DNS}$  denotes the vorticity field computed by Direct Numerical Simulation (DNS), and  $\omega_{POD}$  its truncated projection on the robust POD basis. Specifically, we have

$$\omega_{DNS} = \bar{\omega}(x) + \sum_{i=1}^{\infty} a_i(t) \varphi_i(x) \quad (35)$$

while

$$\omega_{POD} = \bar{\omega}(x) + \sum_{i=1}^{N_R} a_i(t) \varphi_i(x) \quad (36)$$

with  $N_R$  the number of modes retained in the series. Replacing the vorticity in the expression of  $E_\omega$  and making use of the orthonormality of the basis vectors yields:

$$E_\omega^2 = \frac{\sum_{i=N_R+1}^{\infty} a_i^2(t)}{\sum_{i=1}^{N_R} a_i^2(t)}. \quad (37)$$

This represents the fraction of the flow energy which is not represented by the reduced basis, compared to the flow energy in the basis. When the basis is poorly representative of the flow, this measure can then be larger than one, meaning that the reduced basis accounts for less than 50 % of the whole flow energy.

To assess the performance of the robust basis in representing the flow in the range of Reynolds number and control parameter  $\mu$ , we provide in Figure 3 the evolutions of  $E_\omega$  for two flow conditions: flow-1, corresponding to the actual values  $Re = 200$ ,  $\mu = 0.0$ , and flow-2, corresponding to the actual values  $Re = 210$ ,  $\mu = -0.2$ . These flows correspond respectively to the left and right plots in Figure 3. In addition, for a better appreciation of the robust basis performance, the errors are also reported for classical POD bases constructed on deterministic values of  $Re$  and  $\mu$ . Characteristics of these different POD bases are listed in Table 1.

|                  | POD type  | Reynolds            | Control             |
|------------------|-----------|---------------------|---------------------|
| Basis <i>i</i>   | Classical | $Re = 200$          | $\mu = 0.0$         |
| Basis <i>ii</i>  | Classical | $Re = 210$          | $\mu = -0.2$        |
| Basis <i>iii</i> | Classical | $Re = 200$          | $\mu = -0.2$        |
| Basis <i>iv</i>  | Classical | $Re = 210$          | $\mu = 0.0$         |
| Basis <i>v</i>   | Robust    | $Re \in [180, 200]$ | $\mu \in [-0.2, 0]$ |

Table 1

Different POD bases tested. For the robust POD basis, a uniform distribution of  $Re$  and  $\mu$  over their respective range is assumed.

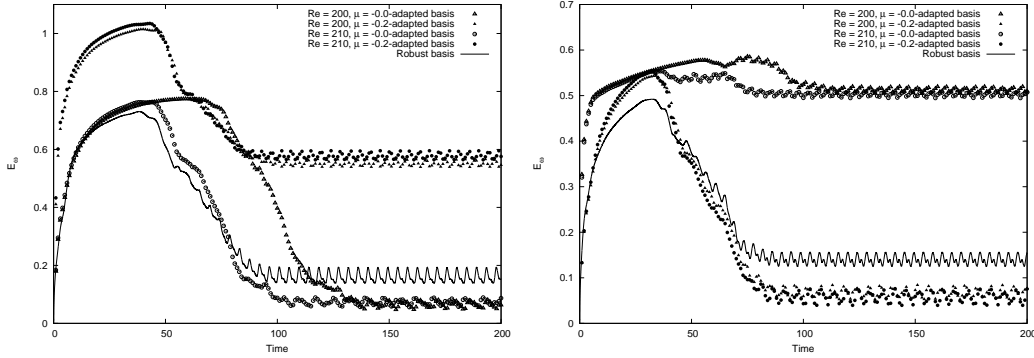


Fig. 3. Representation error  $E_w$  as the wake develops in time from its time-averaged state. Left:  $Re = 200$  flow. Right:  $Re = 210$  flow. Triangles:  $Re = 200$ -flow basis; circles:  $Re = 210$ -flow basis. Open symbols are for a no-blowing flow ( $\mu = 0$ ) while solid symbols are for a maximum suction flow ( $\mu = -0.2$ ). Results from the robust basis are plotted as a solid line.

The representation error is quantified for the different bases and for dynamics off and out of the flow limit-cycle as the basis must be able to represent the flow in a wide range of configurations. Transients as well as asymptotic dynamics are thus considered. The flow is initialized with the time-averaged field and the flow is then let free to develop. At each time step, the flow is projected onto the truncated bases to quantify the energy loss of the different bases. We use  $N_R = 10$  modes for the projection.

Figure 3 shows that for all bases and flow, the errors are initially large before the wake fully develops. This is not a surprise as all the bases are constructed from fully developed flow fields. For the classical POD basis consistent with the actual flow, the error is seen to almost vanish once the wake has fully developed, *i.e.* for  $t \simeq 100$ . For instance, the classical POD basis constructed for  $Re = 200$  and  $\mu = 0$  yields a very low error for  $t > 100$  when the simulated flow indeed corresponds to these conditions ( $Re = 200, \mu = 0$ ) (see Left plot in Figure 3). However, when a classical POD bases is used to project a flow with conditions different than the one use to construct the basis, the error is seen to remain significant even when the flow has developed. For instance, basis *i* does

a poor job representing flow-2, the error stabilizing around 0.5 as  $t$  increases. This clearly illustrates the issue of using non robust POD basis to represent flows in conditions departing to these used for the basis construction.

In contrast, the robust POD basis is seen to achieved acceptable level of error for the two flows (and actually for all flow within the range of  $Re$  and  $\mu$  considered). Specifically, during the transient stage the error for the robust basis is comparable to the errors of the classical POD basis. When the fully developed regime is reach, the error for the robust basis is seen to decrease and level off to a low value. Though larger than the errors for the classical POD bases constructed on the actual flow conditions, the errors for the robust basis are seen to be significantly lower than for inappropriate classical POD bases, and to reach an asymptotic value about 0.15, for all flow conditions. This demonstrate the ability of the robust method to represent flows over a whole range of conditions by relying on a *unique* basis and without requiring any costly correction or updating procedure.

## 4 Optimal control using a robust reduced model

### 4.1 Optimal control basics

We now turn to the control problem, where one seeks for the minimization of the cylinder total drag  $F_D$ , while restraining the control intensity  $\mu(t)$ , and thus the operating cost, from getting too large to remain consistent with real life problems. The control problem is illustrated in Figure 4.

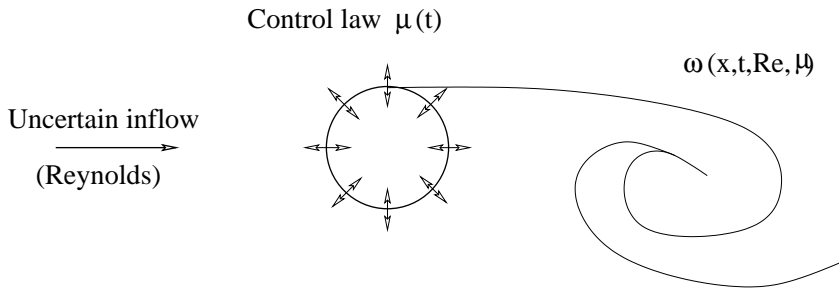


Fig. 4. Sketch of the control problem. The goal is to determine the deterministic control law  $\mu(t)$  (uniform blowing/suction at the cylinder boundary) to minimize the cylinder drag for inflows with uncertain characteristic Reynolds numbers.

This objective is formulated under a cost function form, defined over a time-horizon of length  $T_w$ . In the rest of the paper, we typically considers  $T_w$  corresponding to about 20 vortex-shedding periods of the uncontrolled flow. The control law is a set of time-dependent variables, here considered as vectors. As

the control is the blowing intensity at each time  $t$ , it is however simply noted  $\mu(t)$ .

The cost function writes:

$$\mathcal{J} = \frac{\alpha}{2} \langle \mu; \mu \rangle_{T_w} + \frac{\beta}{2} \langle \langle F_D^2; F_D^2 \rangle \rangle_{T_w}, \quad (38)$$

where the constant  $\alpha > 0$  accounts for the price of the control intensity and  $\beta > 0$  for the cost of the drag force, and  $F_D(u, \mu) \sim U_\infty^2 C_D(u, \mu)$  is the drag force exerted on the cylinder,  $C_D$  being the instantaneous drag coefficient. The bracket term  $\langle \cdot; \cdot \rangle_{T_w}$  here expresses as

$$\langle f; g \rangle_{T_w} = \int_{t_0}^{t_0+T_w} f(t) Q_\diamond g^*(t) dt + c.c..$$

The double-bracket term is

$$\langle \langle f; g \rangle \rangle_{T_w} = \int_{t_0}^{t_0+T_w} f(t) Q_\square g^*(t) dt + c.c.,$$

while  $c.c.$  denotes the complex conjugate and  $*$  is the transconjugate operator.

Operators  $Q_\diamond$  and  $Q_\square$  allow to define the physics one wants to involve in the cost function of the problem. In the current case, the concern is simply about the “energy” of the control  $\mu$ . Further, the drag term is considered in its quadratic form and the operators  $Q_\diamond$  and  $Q_\square$  can hence be chosen as the identity operators  $Q_\diamond \equiv \mathbf{I}$ ,  $Q_\square \equiv \mathbf{I}$ , leading to  $\langle \cdot; \cdot \rangle_{T_w} = \langle \langle \cdot; \cdot \rangle \rangle_{T_w}$ .

We consider the expansion of the flow using the truncated projection of the vorticity field on the robust POD basis  $\{\varphi_i(x)\}_{i=1}^{N_R}$ :

$$\omega(x, t) = \bar{\omega}(x) + \sum_{i=1}^{N_R} a^i(t) \varphi_i(x). \quad (39)$$

Denoting  $a = (a^1, \dots, a^{N_R})$  the POD coefficients of the flow, the reduced model is governed by a state equation:

$$\mathcal{F} \equiv \frac{da}{dt} - F(a, \mu). \quad (40)$$

The Lagrangian of the system expresses as

$$\mathcal{L} = \mathcal{J} - \langle \mathcal{F}; \lambda \rangle_{T_w}, \quad (41)$$

where

$$\langle \mathcal{F}; \lambda \rangle_{T_w} = \int_{t_0}^{t_0+T_w} \left( \frac{da}{dt} - F(a, \mu) \right) \lambda^*(t, \mu) dt + c.c. \quad (42)$$

and  $\lambda(t, \mu)$  the Lagrange multiplier of the state equation.

The Lagrangian now expresses as

$$\begin{aligned} \mathcal{L} = & \int_{t_0}^{t_0+T_w} \left( \frac{\alpha}{2} \mu(t) \mu^*(t) + \frac{\beta}{2} F_D^2(a, \mu) F_D^{2*}(a, \mu) \right) dt \\ & - \int_{t_0}^{t_0+T_w} \left( \frac{da}{dt} - F(a, \mu) \right) \lambda^*(t, \mu) dt + c.c., \end{aligned} \quad (43)$$

where we have substituted the flow field  $u$  with its POD coefficients  $a$  in the expression of the drag force.

When the optimum solution is found, one can show that the Lagrangian function is minimum w.r.t. variations of all the variables and thus locally defines a null linear form. It can further be shown that the stationary points of the Lagrangian are the same as those of the cost function  $\mathcal{J}$  as the term  $\mathcal{F}$  is null for those points and it thus leads to solve the system of equations

$$\frac{d\mathcal{L}}{d\lambda} = 0, \quad \frac{d\mathcal{L}}{da} = 0, \quad \frac{d\mathcal{L}}{d\mu} = 0. \quad (44)$$

After time discretization, one is left with a discrete control vector  $\mu$  which components are the blowing intensity at each time step:  $\mu(i \Delta t) = \mu_i$ . Let  $n_{T_w} = T_w/\Delta t$ ,  $\Delta t$  being the time step. The dimension of the control vector  $\mu$  being  $n_{T_w}$  and generally large, it prevents the use of a linear tangent technique to solve the system (44) and pleads for an adjoint-based approach. As the problem is intrinsically discrete, the definition of the different variable is carefully addressed. In the following, subscript  $k$  denotes the value of the considered variable at time step  $k$  and one uses the following conventions  $t_k = t_0 + (k - 1) \Delta t$ ,  $\forall k \in [1; n_{T_w}]$ :

$$\begin{aligned} a_k &= a(\tau) \text{ for } \tau \in [t_k; t_{k+1}[ , \\ \lambda_k &= \lambda(\tau) \text{ for } \tau \in ]t_{k-1}; t_k], \\ \mu_k &= \mu(\tau) \text{ for } \tau \in [t_k; t_{k+1}[ . \end{aligned}$$

The state equation  $\mathcal{F}(a, \mu) = 0$  is now discrete and is given by

$$\mathcal{F}(a, \mu) = a_{k+1} - \mathcal{M}(a_k, \mu_k) = 0, \quad k \in [1, n_{T_w}], \quad (45)$$

expressing the evolution of the POD coefficients  $a_k$  from time  $t_k$  to time  $t_{k+1}$  through the  $N_R$ -dimensional mapping  $\mathcal{M}$ ; see [14] for details.

Dropping the complex aspect, as all variables are real, and discretizing the

integrals in (Eq. 43) using a standard scheme, one finally gets

$$\mathcal{L} = \sum_{k=1}^{n_{T_w}} \left( \frac{\alpha}{2} \mu_k^2 + \frac{\beta}{2} F_{D_k}^4(a_k, \mu_k) - (a_{k+1} - \mathcal{M}(a_k, \mu_k)) \lambda_{k+1} \right) \Delta t. \quad (46)$$

with  $\lambda_{n_{T_w}+1} = 0$ .

Deriving this expression with respect to  $\lambda_k$  in the Gâteaux sense yields

$$\lim_{\varepsilon \rightarrow 0} \frac{\mathcal{L}(a, \mu, \lambda + \varepsilon \delta \lambda_k) - \mathcal{L}(a, \mu, \lambda)}{\varepsilon} = 0, \quad \forall \delta \lambda_k, k \in [1, n_{T_w}], \quad (47)$$

which reduces to

$$\lim_{\varepsilon \rightarrow 0} \langle \delta \mathcal{F}(a, \mu); \lambda_k \rangle_{T_w} = 0,$$

so one finally recovers the state equation:

$$\mathcal{F}(a, \mu) = 0. \quad (48)$$

Now expressing the derivative w.r.t. the state variable  $a$  gives

$$\lim_{\varepsilon \rightarrow 0} \frac{\mathcal{L}(a + \varepsilon \delta a_k, \mu, \lambda) - \mathcal{L}(a, \mu, \lambda)}{\varepsilon} = 0 \quad \forall \delta a_k, \quad (49)$$

which simplifies in

$$\lim_{\varepsilon \rightarrow 0} \nabla_{a_k} \mathcal{L}(a, \mu) \delta a_k - \langle \lambda; \nabla_{a_k} \mathcal{F}(a, \mu) \delta a_k \rangle_{T_w} = 0,$$

or

$$\beta \langle F_D^2(a, \mu); \nabla_{a_k} F_D^2(a, \mu) \delta a_k \rangle_{T_w} - \langle \nabla_{a_k} \mathcal{F}(a, \mu) \delta a_k; \lambda \rangle_{T_w} = 0,$$

then

$$\beta \langle (\nabla_{a_k} F_D^2(a, \mu)) F_D^2(a, \mu); \delta a_k \rangle_{T_w} - \langle (\nabla_{a_k} \mathcal{F}(a, \mu)) \lambda; \delta a_k \rangle_{T_w} = 0.$$

It finally comes to the so-called adjoint equation:

$$2 \beta (\nabla_{a_k} F_{D_k}) F_{D_k}^3 - \lambda_k + (\nabla_{a_k} [\mathcal{M}(a, \mu)])^\top \lambda_{k+1} = 0. \quad (50)$$

A similar technique for the last derivative term leads to the control optimality equation:

$$2 \alpha \mu_k + 2 \beta (\nabla_{\mu_k} F_{D_k}) F_{D_k}^3 + (\nabla_{\mu_k} [\mathcal{M}(a, \mu)]) \lambda_{k+1} = 0. \quad (51)$$

The solution of the system of equations (Eqs. 48, 50 and 51) leads to the optimal discrete control law  $\mu_k$  and to the direct and adjoint flow fields  $a_k$  and  $\lambda_k$ . This non-linear problem is solved using an iterative Newton technique.

## 4.2 Optimal control results

The optimal control strategy described above is applied to an “ideal” perturbation-free flow where no external disturbance is allowed. This is referred to as the optimal control case. To allow consistent comparisons with the next section, the robust reduced basis is used for the construct the reduced model. That robust basis is derived considering again a Reynolds number and the control intensity uniformly distributed in the respective ranges  $Re \in [180; 220]$  and  $\mu \in [-0.2; 0]$ . The deterministic flow considered for the optimal control results corresponds to  $Re = 200$ . Further, we set the control parameters to:

$$\alpha = 4, \quad \beta = 0.1, \quad n_{T_w} = 180, \quad \Delta t = 0.2.$$

Solving that three-equation system leads to the time-evolution of the optimal blowing/suction  $\mu(t)$  which is the optimal control in the cost function sense (Eq. 38).

The reduced model is first integrated up to its asymptotic regime, with a constant low suction velocity  $\mu = -0.01$ . The control is then turned-on at  $t = 500$ . Once the control is applied, the blowing/suction velocity is seen to drop and to converge to negative values, see Figure 5. A negative blowing velocity means suction and tends to postpone the boundary layers separation on the cylinder surface. As this separation is postponed far beyond the  $\pi/2$ -angle point (with an angle origin at the upstream time-averaged stagnation point), the width of the near wake decreases and it leads to a lower shape drag  $C_P$ . However, sucked boundary layers also induce higher azimuthal velocity radial gradients and thus a higher viscous friction  $C_\nu$ . Those two opposite effects contribute and finally result in a decrease of the total drag. The effect of suction onto the drag is clearly seen in Figure 6, where the total drag coefficient ( $C_D = C_P + C_\nu$ ) is plotted in time, both for the reduced model and the DNS of the flow. For the DNS, the control law computed using the reduced model is imposed as a boundary condition of the Navier-Stokes solver. Figure 7 shows the evolution of the viscous and the pressure drag coefficients for DNS. The optimal control law  $\mu(t)$  determined with the reduced model is then applied to a flow simulated through DNS to quantify its performance in a real system. Quantitative results are gathered in Table 2. While the performance is lower than predicted by the reduced model, due to additional flow details which can not be accounted for by the 10 POD modes, the resulting cost function from in DNS still exhibits a significant decrease, proving that the approach based on controlling the reduced model with a robust basis is applicable and efficient in a full detail-flow context, despite the shortcomings of the method. As described above, the pressure drag decreases when a negative blowing velocity is applied, while the viscous drag increases. Further, while the reduced model

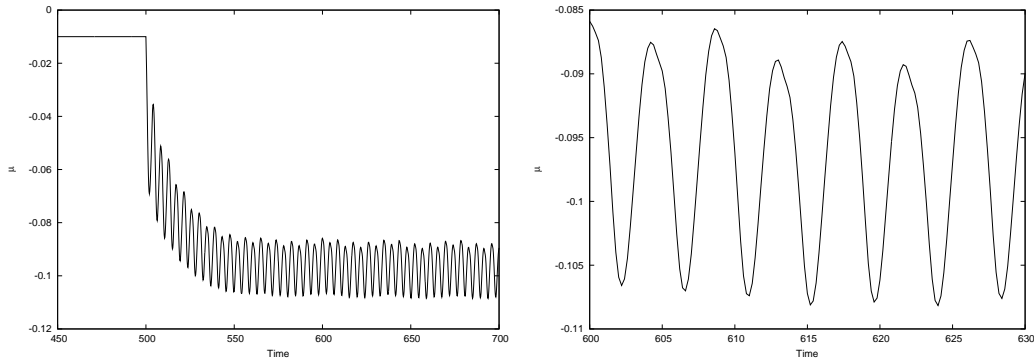


Fig. 5. Control law  $\mu(t)$  for the optimal control scheme, and  $Re = 200$ . Control is turn on at  $t = 500$ .

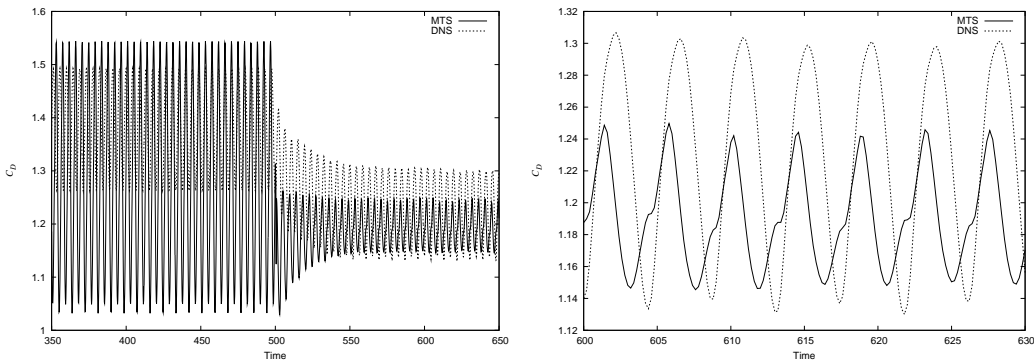


Fig. 6. Total drag history as predicted by the reduced model (labelled MTS) and from DNS of the flow. Control is turned-on at  $t = 500$ .

|              | $\bar{\mu}$ | $\overline{C_{DRED}}$ | $\overline{C_{DDNS}}$ | $\overline{\mathcal{J}_{DNS}}$ |
|--------------|-------------|-----------------------|-----------------------|--------------------------------|
| Uncontrolled | -0.010      | 1.287                 | 1.382                 | 66.45                          |
| Optimal      | -0.091      | 1.191                 | 1.226                 | 47.61                          |

Table 2

Optimal control applied to reduced model (RED) and DNS flows. Over-lined variables denote time-averaged quantities.

is seen to underestimate the amplitude of the time-varying drag oscillations (see Figure 6, right plot), the suction global effect onto the drag evolution is still reasonably well simulated when compared with the DNS prediction. To improve the drag prediction of the reduced model, more modes are to be considered in the robust basis.

Plotting the time evolution of the cost function  $\mathcal{J}$ , in Figure 8, the performance of the control strategy can conveniently be appreciated: it results in a drop of about 30% compared to the non-controlled flow. The absolute performance of the control strategy obviously depends on the choice of the ratio  $\alpha/\beta$  which fix the trade-off between performance and control cost.

The dramatic impact of the control law onto the flow dynamics can best be

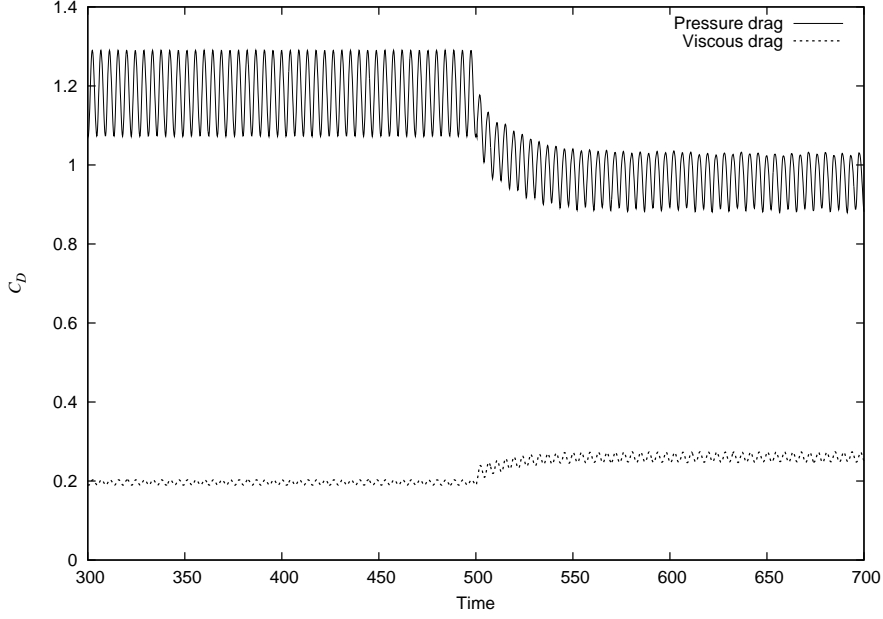


Fig. 7. Pressure and viscous drag time history with DNS.

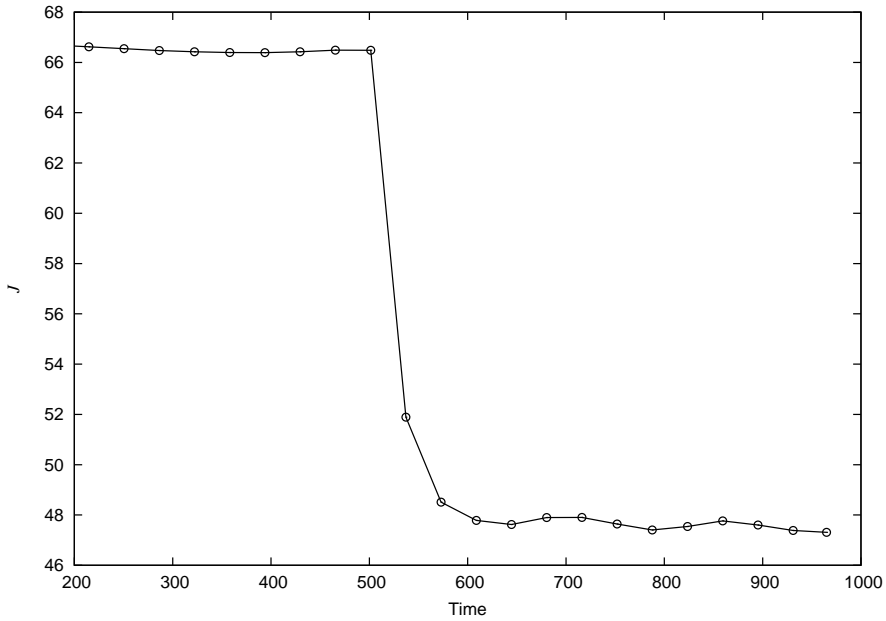


Fig. 8. Objective function  $\mathcal{J}$  with time. Optimal control.

seen in Figure 9, where the evolutions of the first 8 POD coefficients are plotted both in controlled and non-controlled flow configurations. All POD modes dynamics are seen to be affected and to reach a new limit-cycle after a transient period initiated by the sudden control application. For sake of clarity, these transient phase portraits are not plotted. Some coefficients are seen to undergo a dramatic change as they correspond to robust POD modes directly representative of the flow in the immediate vicinity of the cylinder and are thus very sensitive to the local boundary condition along the surface.

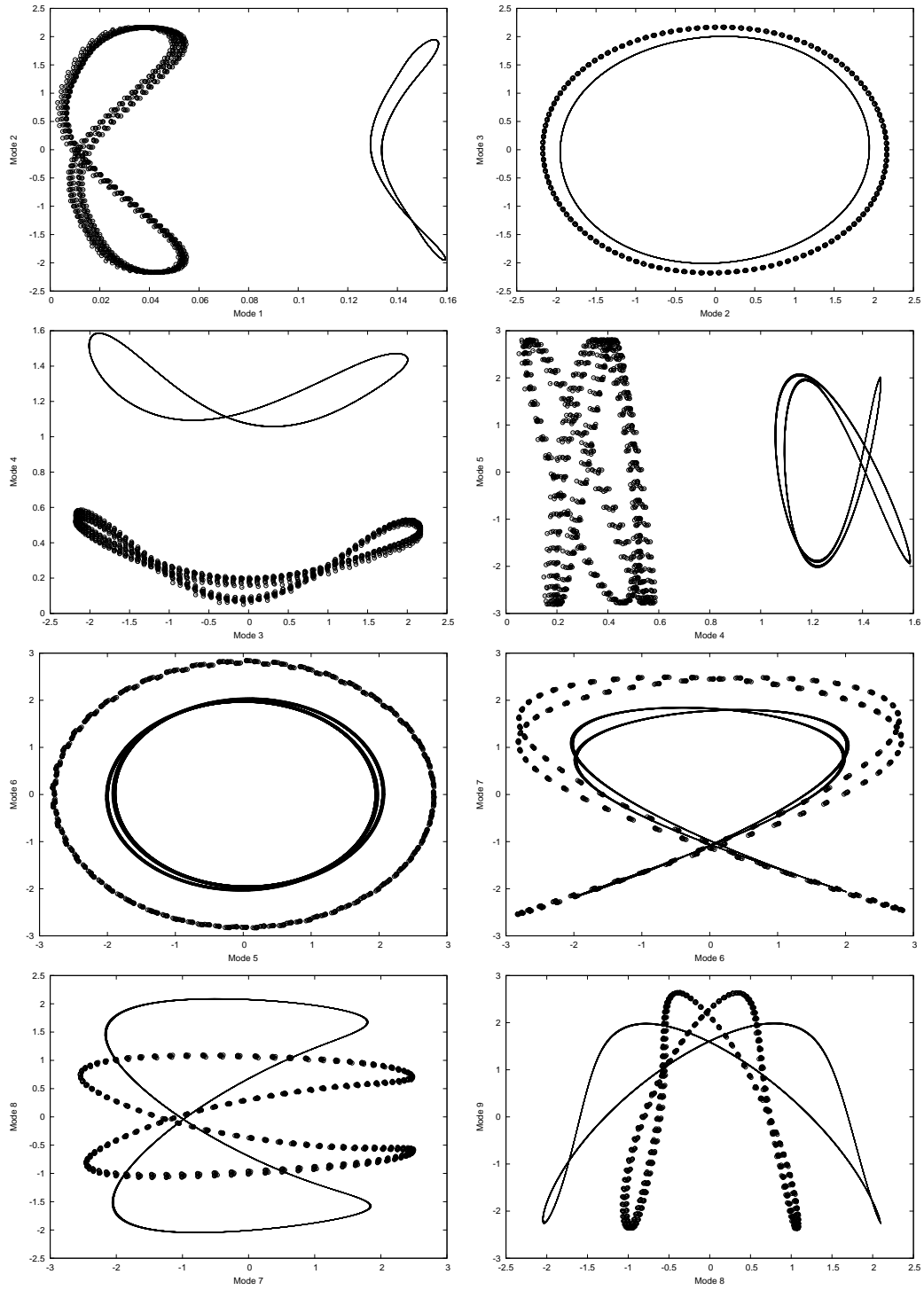


Fig. 9. Projection of the limit-cycles of the POD coefficients of the non-controlled flow (solid lines) and optimally controlled flow (dots).

## 5 Robust control

As seen in Section 2, one can derive a reduced basis which remains valid over a range of flows. In Section 4, we have shown the effectiveness of using a robust basis for the determination of a control strategy in the context of the optimal control theory. In this section, we go one step further and extend the control strategy to situations where the flow is not completely characterized and subjected to external perturbations.

### 5.1 Extended cost function

The flow around the cylinder is assumed to be subjected to uncertainty in the Reynolds number and to unknown external perturbations. Consequently, we seek for a control law that achieves the best performances on average over the assumed range of Reynolds number and which is robust with regards to external perturbations. To this end, the cost function in Eq. (38) is extended to account for unknown perturbations, denoted  $\phi(t)$ , and variability in  $Re$ . Introducing as previously the random Reynolds number of the flow,  $Re(\theta)$ , defined on the probability space  $(\Theta, \mathcal{B}, dP)$ , the extended cost function now writes:

$$\mathcal{J} = \frac{\alpha}{2} \langle \mu; \mu \rangle_{T_w} + \frac{\beta}{2} \langle \langle F_D^2; F_D^2 \rangle \rangle_{T_w} - \frac{\gamma}{2} \langle \phi; \phi \rangle_{T_w}, \quad (52)$$

where the bracket term  $\langle \cdot; \cdot \rangle$  is still expressed as

$$\langle f; g \rangle_{T_w} = \int_{t_0}^{t_0+T_w} f(t) M_{\diamond} g^*(t) dt + c.c.,$$

and the double-bracket term is now

$$\langle \langle f; g \rangle \rangle_{T_w} = \int_{t_0}^{t_0+T_w} \int_{\Theta} f(t, Re(\theta)) M_{\square} g^*(t, Re(\theta)) dP(\theta) dt + c.c.,$$

while  $c.c.$  denotes the complex conjugate and  $*$  is the transconjugate operator.

Without loss of generality the perturbations are here considered to act onto a unique mode of the robust basis, such that  $\phi : t \mapsto \phi(t) \in \mathbb{R}$ . The contribution of the perturbations to the cost function  $\mathcal{J}$  is weighted by the coefficient  $\gamma > 0$ . For  $\gamma \rightarrow \infty$ , one recovers an optimal control strategy where perturbations are not accounted for, but which still account for the randomness in  $Re$ . One is thus left with two optimal parameters  $\mu(t)$  and  $\phi(t)$  to be determined. In the spirit of the  $\mathcal{H}_{\infty}$  approach (see [2] for a brief introduction), the optimal perturbation  $\phi$  leads to the worst-case scenario as it constitutes the most malevolent perturbation to the flow with regards to the cost function  $\mathcal{J}$ .

## 5.2 Robust approach basics

The Reynolds number of the flow being random, so is the flow for given (deterministic) control  $\mu$  and perturbation  $\phi$ . As a result, the state vector  $a$  of the reduced system is also random and the state equation is

$$\frac{da}{dt}(t, \theta) = F(a(t, \theta), \mu(t), \phi(t), Re(\theta)), \quad \forall \theta \in \Theta. \quad (53)$$

With these notations, the Lagrangian of the control problem is

$$\begin{aligned} \mathcal{L} = & \int_{t_0}^{t_0+T_w} \left[ \frac{\alpha}{2} \mu(t) \mu^*(t) - \frac{\gamma}{2} \phi(t) \phi^*(t) \right. \\ & + \int_{\Theta} \frac{\beta}{2} F_D^2(a(t, \theta), \mu(t), \phi(t), Re(\theta)) F_D^{2*}(a(t, \theta), \mu(t), \phi(t), Re(\theta)) dP(\theta) \\ & \left. - \int_{\Theta} \mathcal{F}(a(t, \theta), \mu(t), \phi(t), Re(\theta)) \lambda^*(t, Re(\theta)) dP(\theta) \right] dt + c.c., \quad (54) \end{aligned}$$

where  $F_D$  is the drag force exerted on the cylinder and state equation

$$\mathcal{F}(a, \mu, \phi, Re) \equiv \frac{da}{dt} - F(a, \mu, \phi, Re). \quad (55)$$

The null linear form of the Lagrangian expresses as

$$\frac{d\mathcal{L}}{d\lambda} = 0, \quad \frac{d\mathcal{L}}{da} = 0, \quad \frac{d\mathcal{L}}{d\mu} = 0, \quad \frac{d\mathcal{L}}{d\phi} = 0. \quad (56)$$

As previously, a time discretization of the problem is performed. The discretized form of the state equation (53) is written as

$$a_{k+1}(\theta) = \mathcal{M}(a_k(\theta), \mu_k, \phi_k, Re(\theta)), \quad (57)$$

where the subscript indexes refers to the time level. For the evaluation of the expectation operators in the Lagrangian of the problem, Eq. (54), we again rely on a deterministic cubature formula. Using superscripts to denote the cubature points with associated weights  $w^q$ , Eq. (54) can be recast in:

$$\begin{aligned} \mathcal{L} \simeq & \sum_{k=1}^{n_{T_w}} \left( \alpha \mu_k^2 + \sum_{q=1}^{N_q} w^q \beta F_D^2(a_k^q, \mu_k, \phi_k, Re^q) F_D^{2*}(a_k^q, \mu_k, \phi_k, Re^q) \right. \\ & \left. - \gamma \phi_k^2 - \sum_{q=1}^{N_q} w^q [a_{k+1}^q - \mathcal{M}(a_k^q, \mu_k, \phi_k, Re^q)] (\lambda_{k+1}^q)^* \right) \Delta t. \quad (58) \end{aligned}$$

with  $\lambda_{n_{T_w}+1}^q = 0, \forall q \in [1; n_{T_w}]$ .

Finally, and making use of the fact that all variables are real, conditions (56) leads to the system of equations

$$\left\{ \begin{array}{l} a_{k+1}^q = \mathcal{M}(a_k^q, \mu_k, \phi_k, Re^q), \quad (a) \\ 2\beta \left( \nabla_{a_k^q} (F_D)_{k,q} \right) (F_D^3)_{k,q} - \lambda_k^q \dots \\ \dots + \left( \nabla_{a_k^q} [\mathcal{M}(a_k^q, \mu_k, \phi_k, Re^q)] \right)^\top \lambda_{k+1}^q = 0, \quad (b) \\ 2\alpha \mu_k + \sum_{q=1}^{N_q} w^q \left\{ 2\beta \left( \nabla_{\mu_k} (F_D)_{n,q} \right) (F_D^3)_{k,q} \dots \right. \\ \left. \dots + \left( \nabla_{\mu_k} [\mathcal{M}(a_k^q, \mu_k, \phi_k, Re^q)] \right) \lambda_{k+1}^q \right\} = 0, \quad (c) \\ 2\alpha \phi_k + \sum_{q=1}^{N_q} w^q \left\{ 2\beta \left( \nabla_{\phi_k} (F_D)_{n,q} \right) (F_D^3)_{k,q} \dots \right. \\ \left. \dots + \left( \nabla_{\phi_k} [\mathcal{M}(a_k^q, \mu_k, \phi_k, Re^q)] \right) \lambda_{k+1}^q \right\} = 0. \quad (d) \end{array} \right. \quad (59)$$

In this equations, we have used the short-hand notation  $(F_D)_{k,q}$  for  $F_D(a_k^q, \mu_k, \phi_k, Re^q)$ . The resolution of this system of equations yields the discrete  $Re$ -averaged optimal ( $\gamma \rightarrow \infty$ ) or robust ( $\gamma < \infty$ ) control law  $\mu_k$ , for the most malevolent perturbation  $\phi_k$ .

Below, we provide an outline of the algorithm used for the resolution and application of the robust control strategy.

- (1) Initialize the flow state vector  $a(t=0)$  (*i.e* set  $a_{k=0}$ ).
- (2) Set guessed control law  $\mu_k$  and optimal perturbation  $\phi_k$ , for  $k = 0, \dots, N_{T_w}$  (for instance solution at previous time-horizon).
- (3) For each of the Reynolds values corresponding to the cubature points: solve for state vector  $a_k^q$  and adjoint solution  $\lambda_k^q$ , from (59,a-b) using the current guessed control law  $\mu_k$ , optimal perturbation  $\phi_k$ , and same initial condition  $a_{k=0}^q = a_{k=0}$ ,  $\forall q$ .
- (4) Solve (59,c-d) using previous  $a_k^q$  and  $\lambda_k^q$ , to yield new guessed for the control law  $\mu_k$  and optimal perturbation  $\phi_k$ , for  $k = 0, \dots, N_{T_w}$ .
- (5) Check convergence of the guessed control law. If not converged then repeat from step (3).
- (6) Advance in time the system state vector  $a_k$ ,  $k = 1, \dots, N_{T_w}$  using the state equation (57) with the actual Reynolds number of the flow ( $Re_0$ ) and the control law obtained at the previous step and null perturbation  $\phi_k = 0$ .
- (7) Repeat from step (2), for the next time horizon, using  $a_{k=N_{T_w}}$  as the new initial condition for the state vector:  $a_0 \leftarrow a_{N_{T_w}}(Re_0)$ .

## 6 Results

In this section, we provide a comparison of the respective efficiencies of the control laws  $\mu(t)$  obtained for different control strategies and applied to different flow conditions, *i.e.* flow with different Reynolds numbers. All the control laws are computed on the reduced model using the robust basis, derived by assuming  $Re \in [180; 220]$  and  $\mu \in [-0.2 : 0]$  with uniform distribution. Three control strategies are compared:

- **Optimal-200**: the control law obtained for the optimal theory and based on the assumption of  $Re = 200$  for the flow, and no perturbation ( $\gamma \rightarrow \infty$ ). This strategy follows the derivation of Section 4.
- **Robust**: the control law obtained for the optimal theory (*i.e.* without external perturbations,  $\gamma \rightarrow \infty$ ) but assuming a Reynolds number uniformly distributed in the range  $[180, 220]$ .
- **Robust- $\mathcal{H}_\infty$** : the control law obtained assuming a Reynolds number uniformly distributed in the range  $[180, 220]$  *and* external perturbation on mode 3 of the robust basis ( $\gamma < \infty$ ).

Unless otherwise stated, the control parameters are set to

$$\alpha = 4, \quad \beta = 0.1, \quad \gamma = 50, \quad N_q = 7, \quad \Delta t = 0.2.$$

In every experiments, the reduced model is first run for 500 units of time with actual Reynolds number to obtain an established flow. For a given control strategy, the control law  $\mu(t)$  is then computed over the next  $T_w$  units of time. This control law is then applied to the reduced model, for again the actual value of the Reynolds number of the flow, providing the updated model state. The procedure is subsequently repeated for the next  $T_w$  unit of time and so on.

The evolutions of the control intensity  $\mu(t)$  obtained for the three different strategies and  $T_w = 36$  units of time are plotted in Figure 10. The actual Reynolds number of the flow is  $Re = 200$ . It is seen that, though close, the robust formulation leads to a larger control intensity compared to the optimal-200 strategy. Indeed, the drag force exerted onto the cylinder varies in a non-linear way in the assumed Reynolds range, so the resulting drag force in the ensemble average sense tends to be higher than the drag force for  $Re = 200$ , with higher control law as a result. In fact, we have:

$$\langle \langle F_D(a, \mu, \phi, Re) \rangle \rangle_{T_w} > \langle F_D(a, \mu, \phi, Re = 200) \rangle_{T_w}. \quad (60)$$

When external optimal perturbations  $\phi$  are considered, they tend to increase both the drag and the cost function. The control intensity leading to the best

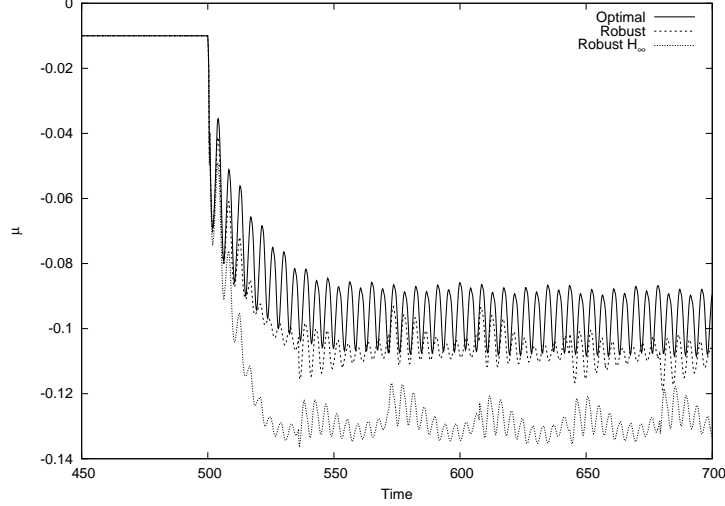


Fig. 10. Control laws for the the different control strategies.

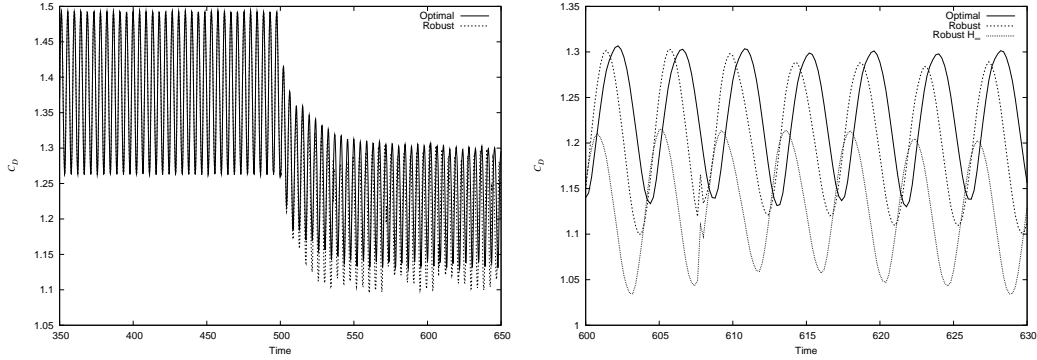


Fig. 11. Total drag evolution in presence of control. Reduce model,  $Re = 200$ .

compromise between drag and control intensity is then significantly larger to counterbalance this adverse effect.

The resulting drag time-evolution of the controlled flow at  $Re = 200$ , as estimated by the reduced model, is plotted in Figure 11 for the three control strategies. When the control is applied, the drag time-evolution from the different strategies all show a sharp decrease in their mean value. The lowest drag is achieved for the robust- $\mathcal{H}_\infty$  strategy while the optimal control is less efficient. This is consistent with the control laws intensity shown above. Table 3 presents the quantitative results, both from the reduced model estimates and for the computed control laws applied to the DNS of the flow at  $Re = 200$ . It shows the time-averaged drags as well as the cost function achieved for the DNS flow. As the flow is deterministic, the performances of the control is investigated here in terms of  $\mathcal{J}_{det}$ , the objective function evaluated for a deterministic Reynolds number, *i.e.* considering  $\langle\langle\cdot\rangle\rangle_{T_w} = \langle\cdot\rangle_{T_w}$ . As in the preceding section, the control law determined for the reduced model remains relevant when applied to a (real) DNS flow and achieves a significant decrease of the drag.

|                             | $\bar{\mu}$ | $\overline{C_{DRed}}$ | $\overline{C_{DDNS}}$ | $\overline{\mathcal{J}_{det,DNS}}$ |
|-----------------------------|-------------|-----------------------|-----------------------|------------------------------------|
| Uncontrolled                | -           | 1.287                 | 1.382                 | 69.45                              |
| Optimal-200                 | -0.097      | 1.191                 | 1.226                 | 51.01                              |
| Robust                      | -0.107      | 1.178                 | 1.201                 | 49.00                              |
| Robust $\mathcal{H}_\infty$ | -0.129      | 1.151                 | 1.131                 | 44.08                              |

Table 3

Performance of the different control strategies, in terms of mean drag (estimated from the reduced model  $\overline{C_{DRed}}$  and computed in DNS  $\overline{C_{DDNS}}$ ) and cost function  $\mathcal{J}_{det}$  in DNS assuming the actual value of the Reynolds number  $Re = 200$ .

Discontinuities can be observed in the temporal evolution of the control law and resulting drag in Figures 10 and 11, for instance at  $t = 536$ . This occurs at the interface between two successive control laws. It is due to the re-initialization of the random flow state to the state for the actual flow, *i.e.* for  $Re = 200$ , before determining the subsequent control laws following the robust strategies. In other words, the initial condition on the random state vector  $a(t, \theta)$  is always reset to the deterministic state at  $t$  before treating the next time span.

### 6.1 Performance evaluation

To investigate the robust character of the control, its performance for different Reynolds number flows is plotted in Figure 12. The performance is here measured against the reduced model, for flows at several actual Reynolds numbers in the assumed range [180 : 220] and the different control strategies. The performance is measured from the robust objective function at the actual flow Reynolds. Comparison of efficiency is made for the following control strategies: robust, robust- $\mathcal{H}_\infty$ , optimal (assuming  $Re = 200$ ) and optimal-deterministic (assuming the actual Reynolds number).

As expected, the deterministic control law yields the best performance for all  $Re$  as it is optimal and uses the actual Reynolds number. The optimal strategy determined assuming  $Re = 200$  performs equally well when the actual Reynolds is indeed equal to 200, but is significantly less efficient when applied to flows with actual Reynolds numbers different from 200. The control laws for the robust strategies, though always less efficient than the deterministic laws, yield a better efficiency on average over the Reynolds range compared to the optimal law  $Re = 200$ . For a better appreciation of the respective performances at the different Reynolds numbers, we have plotted in Figure 13 the differences in the resulting objective cost functions, relatively to the optimal deterministic law using the actual  $Re$ . It shows the advantage of accounting for a variability in flow conditions when deriving the control law. When also accounting for

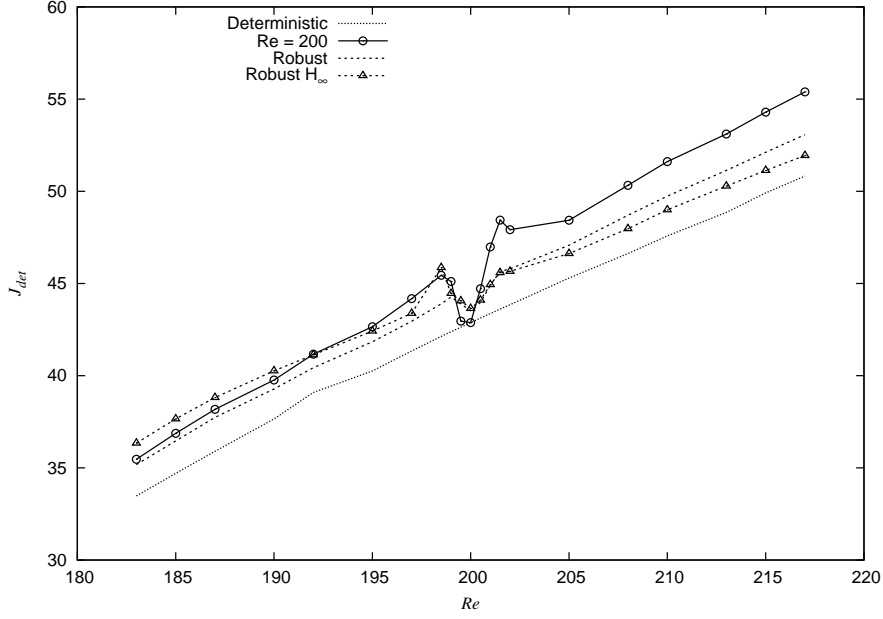


Fig. 12. Achieved cost functions for different control strategies as a function of the actual flow Reynolds number. Cost functions are based on the reduced model estimation.

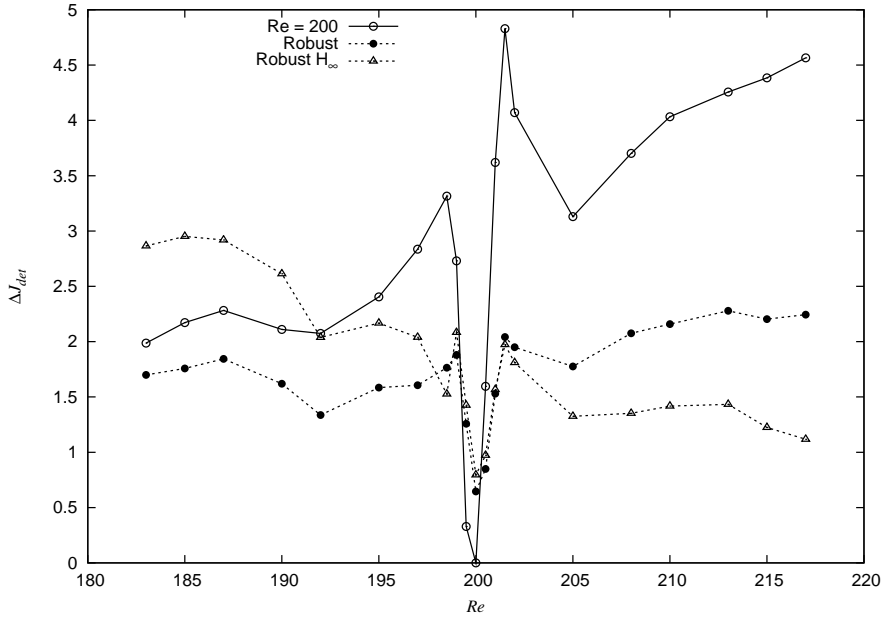


Fig. 13. Performance loss, relatively to optimal controls based on the actual  $Re$ , of the different control strategies as a function of the actual flow Reynolds number. Performances are measured using reduced model estimates of the cost functions.

finite energy external perturbation, the robust- $\mathcal{H}_\infty$  control leads to trends similar as the robust control while achieving a more constant performance in the  $Re$  range: it gives poor performance at low  $Re$ , achieving an even worse objective cost than the  $Re = 200$ -optimal control, but performs very well for the larger  $Re$ .

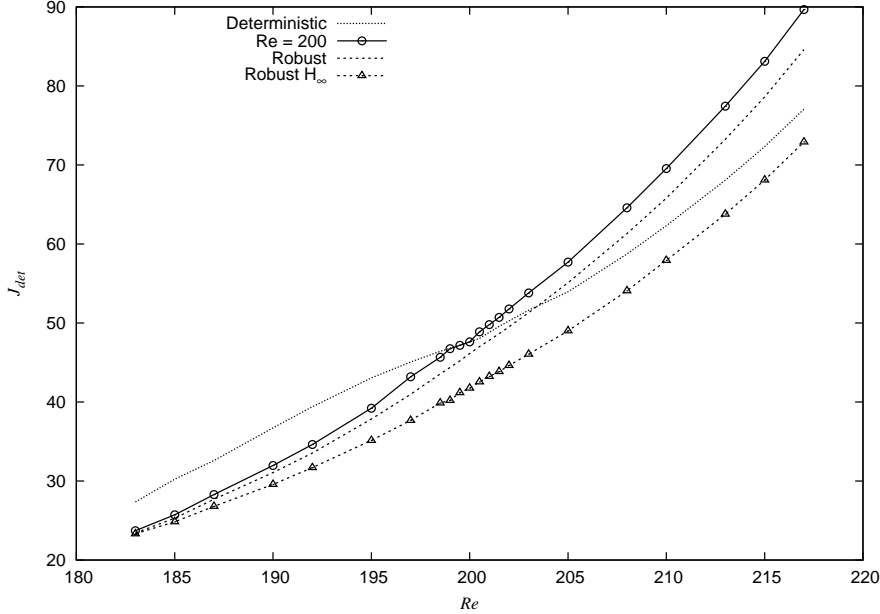


Fig. 14. DNS estimates of the cost function for the different control laws as a function of the actual Reynolds number of the flow.

|                             | $\mathcal{J}_{Red}$ | $\eta_{Red}$ | $\mathcal{J}_{DNS}$ | $\eta_{DNS}$ |
|-----------------------------|---------------------|--------------|---------------------|--------------|
| Deterministic               | 42.64               | 0.0 %        | 49.52               | 0.0 %        |
| Optimal-200                 | 45.08               | 5.7 %        | 51.01               | 3.0 %        |
| Robust                      | 44.23               | 3.7 %        | 49.00               | -1.0 %       |
| Robust $\mathcal{H}_\infty$ | 44.28               | 3.8 %        | 44.08               | -11.0 %      |

Table 4

Comparison of performance achieved for different control strategies. Robust objective function  $\mathcal{J}$  and relative “losses”  $\eta$  (compared to optimal laws for actual  $Re$ ).  $Red$  and  $DNS$  denote measures using the reduced model or the flow DNS.

The previous experiments use the reduce model for both the control law determination and performance measurement. To assess the robustness of the control laws, they are now applied to the DNS of the flow. Performances, again in terms of the cost functions but computed from the DNS solutions, are monitored and plotted in Figure 14. Figure 15 shows the difference in performances with regard to the optimal law determined using the actual flow Reynolds number. Unlike the prediction of the reduced model, the robust- $\mathcal{H}_\infty$  control law is here seen to provide the best performance of all strategies when applied to the DNS flow for all Reynolds numbers. Second in terms of performance is the robust control while the  $Re = 200$ -control performs better than the deterministic control in the lower part of the Reynolds number range considered. These results stress the importance of the reduced model quality and the need to account for robustness when designing a control law.

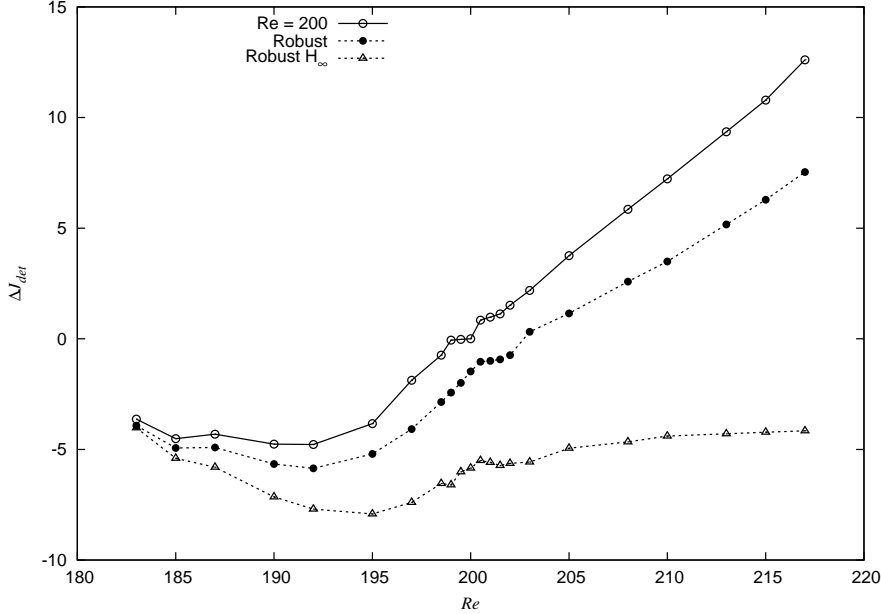


Fig. 15. DNS estimates of the difference in cost function relatively to optimal controls based on the actual  $Re$ , of the different control strategies as a function of the actual flow Reynolds number.

The performance averaged over the Reynolds range  $[180; 220]$  are gathered in Table 4. For the reduced model, the expected results are obtained: in this perturbation-free framework, while the deterministic control performs best and the optimal control performs worst, the robust control achieves a (slightly) better performance than the robust- $\mathcal{H}_\infty$  approach which has to account for potential perturbations. Results are significantly different when the control laws are applied in the DNS of the flow: the robust- $\mathcal{H}_\infty$  averaged performance is much better than that of the robust approach (with no  $\phi$  perturbation). Accounting for the most malevolent perturbation in the reduced model thus increases the control performance determined from a low-fidelity model when applied to a high-accuracy simulation code. This is believed to be a fundamental point as it gives rules of thumb for an accurate and consistent application of the reduced model-based robust control strategy.

## 6.2 Influence of the time-horizon

As the cost function  $\mathcal{J}$  is defined over a time-horizon of length  $T_w$ , it is necessary to investigate how the selection of  $T_w$ s affects the resulting control performance. Figure 16 shows the control laws derived from  $n_{T_w} = 90, 180$  and  $360$ . Focusing on the  $n_{T_w} = 360$ , it is seen to feature large oscillations at the beginning of the horizon that subsequently decay almost to zero amplitude for later times. A similar trend is seen for  $n_{T_w} = 180$  while for  $n_{T_w} = 90$ , the time-horizon is too short to observe the decay of the oscillations. This

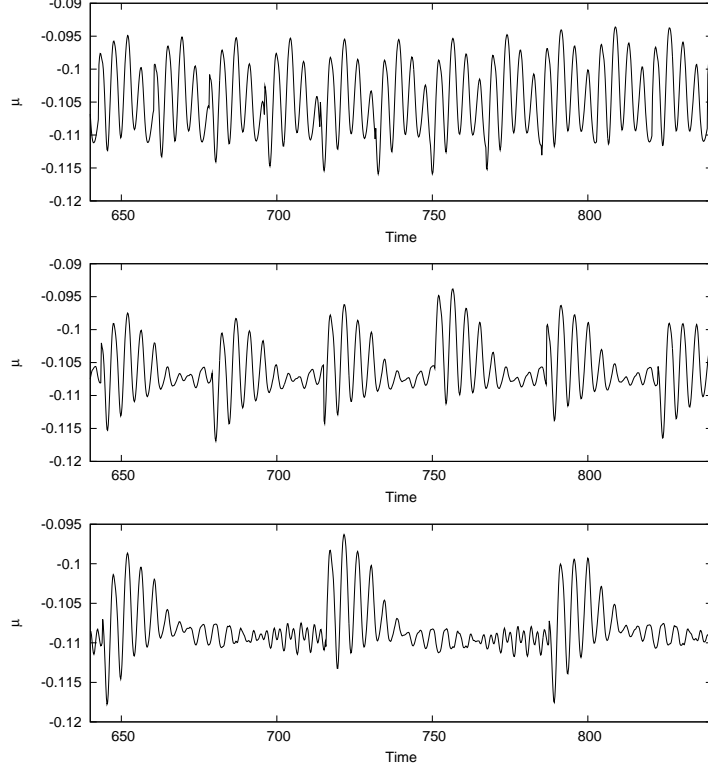


Fig. 16. Robust control law for different time-horizons  $T_w = n_{T_w} \Delta t$ . From top to bottom,  $n_{T_w} = 90, 180$  and  $360$ .

|                            | $\overline{\mathcal{J}}_{rob,Red}$ | $\eta_{rob,Red}$ | $\overline{\mathcal{J}}_{rob,DNS}$ | $\eta_{rob,DNS}$ |
|----------------------------|------------------------------------|------------------|------------------------------------|------------------|
| Deterministic              | 42.64                              | 0.0 %            | 49.52                              | 0.0 %            |
| Robust ( $n_{T_w} = 90$ )  | 44.42                              | 4.2 %            | 49.32                              | -0.4 %           |
| Robust ( $n_{T_w} = 180$ ) | 44.23                              | 3.7 %            | 49.00                              | -1.0 %           |
| Robust ( $n_{T_w} = 360$ ) | 44.20                              | 3.7 %            | 48.54                              | -2.0 %           |

Table 5

Comparison of the performance for different control time-horizons  $T_w = n_{T_w} \Delta t$ . Robust objective function  $\mathcal{J}_{rob}$  and relative “losses”  $\eta$  compared to a deterministic approach.

behavior is again explained by the re-initialization of the random flow state to the deterministic actual flow state at the beginning of the time horizon. Still, when uncertainty in the Reynolds number is accounting for, the random flow evolves with different phase velocities: while initially in phase, different flow realizations becomes out of phase after some time. As a result, the Reynolds average control law loses phase information and tends to become constant as time advances. However, in terms of performance the longer the time horizon the better the cost function achieved as may be appreciated from Table 5.

## 7 Concluding remarks

In this paper, a new technique for the derivation of a robust POD basis for a flow has been proposed. The robustness is sought to improve the representation properties of the basis in a given range of flow parameters. The efficiency of the robust basis was tested and compared successfully with the classical POD basis, for the representation of the flow over a circular cylinder in laminar regime. The robust basis was then used on a reduced model of the flow to determine the optimal control law for reducing the drag of the cylinder. The control law derived for the reduced model was then applied to a DNS of the flow with satisfactory results.

The optimal control strategy was subsequently extended to account for some uncertainties in the Reynolds number of the flow. The control law is then sought to achieve the minimum of a cost function on average over a specified range of flow conditions (Reynolds number). It yields two robust control strategies depending on the account for some external perturbations. When applied to the reduced model, these strategies yield control laws that are indeed more efficient on average than the optimal strategy based on the expected flow conditions. Further, when the control laws are used in a DNS of the flow, the performance of the robust controls are found to be always better than the deterministic optimal control found for the reduced model for the actual flow conditions.

These results highlight the importance of using a robust basis in the reduced model to be able to account for significant changes in the flow structure as the control law is applied in uncertain flow conditions. The incorporation of operational uncertainty and external perturbation (to account for model reduction error) when deriving an open-loop flow control strategy, is seen to significantly improve the control performance when applied to the non-reduced system.

## References

- [1] BERGMANN M., CORDIER L. & BRANCHER J.-P., Optimal rotary control of the cylinder wake using POD reduced order model, *Phys. Fluids*, **17**(9), 2005.
- [2] BEWLEY T.R., Flow control: new challenges for a new Renaissance, *Prog. Aero. Sci.*, **37**, p. 21-58, 2001.
- [3] BUI-THANH T., DAMODARAN M. & WILLCOX K., Proper orthogonal decomposition extensions for parametric applications in transonic aerodynamics, *AIAA Paper 2003-4213*, 2003.

- [4] BURKARDT J., GUNZBURGER M. & LEE H.-C., Centroidal Voronoi tessellation-based reduced-order modeling of complex systems, to appear in *SIAM J. Scien. Comput.*
- [5] CAMERON R.H. & MARTIN W.T., The orthogonal development of nonlinear functionals in series of Fourier-Hermite functionals, *Ann. Math.*, **48**, p. 385-392, 1947.
- [6] CHRISTENSEN E.A., SØRENSEN J.N., BRONS M. & CHRISTIANSEN P.L., Low-dimensional representations of early transition in rotating fluid flow, *Theoret. Comput. Fluid Dynamics*, **5**, p. 259-267, 1993.
- [7] CONN A.R., GOULD N.I.M., TOINT P.L., *Trust-region methods*, MPS/SIAM series on optimization, 951 p., 2000.
- [8] GALLETTI B., BRUNEAU C.H., ZANNETTI L. & IOLLO A., Low-order modelling of laminar flow regimes past a confined square cylinder, *J. Fluid Mech.*, **503**, p. 161-170, 2004.
- [9] GERHARD J., PASTOOR M., KING R., NOACK B.R., DILMANN A., MORZYŃSKI M. & TADMOR G., Model-based control of vortex shedding using low-dimensional Galerkin models, *33<sup>rd</sup> AIAA Fluids Conf. & Exhibit*, AIAA 2003-4262, Orlando, FL, June 23-26, 2003.
- [10] GHANEM R.G. & SPANOS P.D., *Stochastic finite elements: a spectral approach*, Springer Verlag, 1991.
- [11] GUNES H. & RIST U., Proper orthogonal decomposition reconstruction of a transitional boundary layer with and without control, *Phys. Fluids*, **16**(8), p. 2763-2784, 2004.
- [12] HOLMES P., LUMLEY J.L. & BERKOOZ G., *Turbulence, coherent structures, dynamical systems and symmetry*, Cambridge University Press, 420 p., 1996.
- [13] LE MAÎTRE O., SCANLAN R. H. & KNIO O. M., Estimation of the flutter derivatives of an NACA airfoil by means of Navier-Stokes simulation, *J. Fluids Struct.*, **17**(1), p. 1-28, 2003.
- [14] LE MAÎTRE O. & MATHELIN L., Fluid flow simulation using a reduced model coupled with polynomial chaos expansions, submitted, 2007.
- [15] LE MAÎTRE O., REAGAN M.T., KNIO O.M., NAJM H.N. & GHANEM R.G., A stochastic projection method for fluid flow. I. Basic formulation, *J. Comput. Phys.*, **173**(2), p. 481-511, 2001.
- [16] LE MAÎTRE O., REAGAN M.T., KNIO O.M., NAJM H.N. & GHANEM R.G., A stochastic projection method for fluid flow. II. Random process, *J. Comput. Phys.*, **181**(1), p. 9-44, 2002.
- [17] LUMLEY J.L., The Structure of Inhomogeneous Turbulent Flows, In *Atmospheric turbulence and radio propagation*, edited by A.M. Yaglom and V.I. Tatarski, Moscow: Nauka, p.166-178, 1967.

- [18] MA X. & KARNIADAKIS G.E., A low-dimensional model for simulating three-dimensional cylinder flow, *J. Fluid Mech.*, **458**, p. 181-190, 2002.
- [19] MATHELIN L., HUSSAINI M.Y., ZANG T.A. & BATAILLE F., Uncertainty propagation for turbulent, compressible nozzle flow using stochastic methods, *AIAA Journal*, **42**(8), p. 1669-1676, 2004.
- [20] MATHELIN L., HUSSAINI M.Y. & ZANG T.A., Stochastic approaches to uncertainty quantification in CFD simulations, *Num. Algo.*, **38**(1), p. 209-236, 2005.
- [21] MORZYŃSKI M., STANKIEWICZ W., NOACK B.R., THIELE F. & TADMOR G., Generalized mean field model for flow control using a continuous mode interpolation, *3rd AIAA Flow Control Conference*, AIAA paper 2006-3488, 2006.
- [22] NOACK B.R., AFANASIEV K., MORZYŃSKI M., TADMOR G. & THIELE F., A hierarchy of low-dimensional models for the transient and post-transient cylinder wake, *J. Fluid Mech.*, **497**, p. 335-363, 2003.
- [23] NOVAK E. & RITTER K., Simple cubature formulas with high polynomial exactness, *Constructive approximation*, **15**, p. 499-522, 1999.
- [24] PARK H.M., LEE M.W. & JANG Y.D., An efficient computational method of boundary optimal control problems for the Burgers equation, *Comput. Methods. Appl. Mech. Engrg.*, **166**, p. 289-308, 1998.
- [25] PETRAS K., Fast calculation of coefficients in the Smolyak algorithm, *Num. Algo.*, **26**, p. 93-109, 2001.
- [26] PETRAS K., Asymptotically minimal Smolyak cubature, preprint, [<http://www-public.tu-bs.de:8080/~petras/software.html>].
- [27] PRABHU R.D., SCOTT COLLIS S. & YONG CHANG, The influence of control on proper orthogonal decomposition of wall-bounded turbulent flows, *Phys. Fluids*, **13**(2), p. 520-537, 2001.
- [28] RAVINDRAN S.S., A reduced-order approach for optimal control of fluids using proper orthogonal decomposition, *Int. J. Numer. Meth. Fluids*, **34**, p. 425-448, 2000.
- [29] REMPFER D., Investigations of boundary layer transition via Galerkin projections on empirical eigenfunctions, *Phys. Fluids*, **8**(1), p. 175-188, 1996.
- [30] SIROVICH L., Turbulence and the dynamics of coherent structures. Part 1: coherent structures, *Quarterly of Applied Mathematics*, **45**(3), p. 561-571, 1987.
- [31] SMOLYAK S.A., Quadrature and interpolation formulas for tensor product of certain classes of functions, *Dokl. Akad. Nauk SSSR*, **4**, p. 240-243, 1963.
- [32] TANG K.Y., GRAHAM W.R. & PERAIRE J., Active flow control using a reduced order model and optimum control, *AIAA Paper 96-1946*, 1996.

- [33] WIENER S., The homogeneous chaos, *Amer. J. Math.*, **60**, p. 897-936, 1938.
- [34] XIU D.B. & KARNIADAKIS G.E., Modeling uncertainty in steady state diffusion problems via generalized polynomial chaos, *Comput. Methods Appl. Mech. Engrg.*, **191**, p. 4927-4948, 2002.